Rheology, simulation and data analysis toward bioprinting cell viability awareness

Marquette Christophe, Lucas Lemarié, Aravind Anandan, Emma Petiot, Christophe Marquette, Edwin-Joffrey Courtial

Journal: Bioprinting

Type of article: Original research

Title:

Rheology, simulation and data analysis toward bioprinting cell viability awareness.

***Authors**:*

LEMARIÉ Lucas[1], ANANDAN Aravind[1], PETIOT Emma[1], MARQUETTE Christophe[1] and COURTIAL Edwin-Joffrey[1]

Affiliation:

[1]3d.FAB, Univ Lyon, Université Lyon1, CNRS, INSA, CPE-Lyon, ICBMS, UMR 5246, 43, Bd du 11 novembre 1918, 69622 Villeurbanne cedex, France

Corresponding author: edwin.courtial@univ-lyon1.fr

Keywords: Bioprinting, Cells Viability, Shear stress, Time, Rheology, Bioink

Abstract: Microextrusion-based bioprinting consists of extruding a cellularized hydrogel through a nozzle of known geometry. As a consequence of this travelling through the nozzle, shear forces will inevitably be generated upon cells during the extrusion process and have a negative effect on cell viability, proliferation and biological fate of the tissue. In the present study and for the first time in the bioprinting field, flow simulation and cells fate (lysis, necrosis, apoptosis and viable) were consolidated to establish mathematical relationships. We demonstrated that for

constant residence time at wall, the higher the wall shear stress values, the lower the viable populations. Furthermore, at constant maximum wall shear stress, the longer the residence time at wall, the lower the viable populations. Regarding the quantification of the damaged fibroblasts (lysis, necrosis and apoptosis) during the microextrusion, lysis was shown to be the prevailing cell death pathway compared to necrosis and apoptosis. Finally, partial least square (PLS) modelling was able to correctly predicted viable cells' population with a high correlation (R^2 of 0.859; error of 9.2%) between predicted and measured viable cells percentage. This model was shown to be predictive over a large range of cells viability (38.5 – 94%) with a prediction error of only 9.2%.

1. Introduction

Bioprinting is a cell-based additive manufacturing process becoming increasingly popular in the tissue engineering field [1,2]. The technique enables researchers to create mono- or multi-cell tissues for medical and pharmacological applications [3–5]. Thus, at the heart of the biotechnology field, bioprinting holds great promises for regenerative medicine, especially for the autograft production [6,7]. According to the final application and the required printing resolution, several technologies were developed such as inkjet, microextrusion, laser-assisted or stereolithography-based bioprinting [8].

Among all these bioprinting techniques, when it comes to cell density fine tuning [9,10] and fabrication of physiologically relevant tissue [11], microextrusion (also called liquid deposition modelling or extrusion based bioprinting [12]) appears as the most efficient technology[13]. It is indeed the only one able to offer the possibility to control precisely bioinks cellular density while printing human size complex living objects.

Microextrusion-based bioprinting consists of extruding a cellularized hydrogel (also called bioink) through a nozzle of known geometry, most of the time with diameter in the 100-800 µm range [11]. As a consequence of this travelling through the nozzle, shear forces will inevitably be generated upon cells during the extrusion process [14,15]. The magnitude of these forces depending on the bioink rheological behaviour [16,17] which can be tailored by temperature [18], cartridge size, nozzle geometry but also by the flow rate applied to performed the extrusion [12,17,19]. Out of these forces, shear stress generated during bioprinting was recently described to have a negative effect on cell viability, proliferation and biological fate of the tissue [16]. The survival or viability rate was thus shown to be impaired [17] by shear stress affecting membrane integrity [20], leading then to cell lysis and in a lower extent to cell necrosis[21]. Understand and predict the cell-stress relationship is then mandatory in order to ensure viability and proper recapitulation of the growing tissue functions.

It has also been demonstrated that cell mechanical environment plays an essential role upon cell structure and function[22]. An example of this role is the effect of the shear stress applied to endothelial cells which promotes atheroprotective factors releasing and further inhibition of coagulation by mechanochemical transduction. Nevertheless, these mechanical stimulations shall be finely controlled since acute

stress levels were also shown to lead to endothelial surface degeneration, erosion, and limitation of cell division capacity[23].

In the present work, cell-stress relationship during microextrusion was investigated, simulated and characterized both quantitatively and qualitatively. Skin fibroblasts were used as a cellular model [14], seeded within a previously described hydrogel formulation [7]. Computational Fluid Dynamics (CFD) simulations were performed in order to predict flow velocity within different nozzle geometries. The corresponding shear stress values were calculated using an in-house developed code and the quantification of their impact on fibroblast lysis, necrosis and apoptosis, allowed us to complement and go a step further than the previously published studies[14,21,24,25]. Finally, a partial least square (PLS) modelling approach was applied to the obtained data set in order to demonstrate the clear relationship between cell fate and bioprinting conditions, leading to the achievement of a predictive mathematical model.

2. Materials and methods

2.1 Cell culture of human dermal fibroblasts

Foreskin samples were obtained from healthy patients with written informed consent. Surgical residues were harvested according to French regulation including declaration to research ministry (DC No. 2014- 2281). Fibroblasts were isolated and cultivated in T75 flasks at 37°C, 5% CO_2 in Dulbecco's Modified Eagle Medium (DMEM)/Glutamax (Gibco Cell Culture, Invitrogen, France), supplemented with 10% (v/v) calf bovine serum (Gibco Cell Culture, Invitrogen, France), 0.5% (v/v) amphotericine B (Gibco Cell Culture, Invitrogen, France) and 1% Penicillin/Streptomycin [26]. Cells were subcultured once a week for passaging until microextrusion bioprinting.

2.2 Bioink formulation and cell seeding

Bioinks were prepared according to the formulation described by Pourchet and al.[7]. They were composed of bovine gelatin (Sigma-Aldrich, France), very low viscosity alginate (Alpha Aesar, France) and fibrinogen (Sigma-Aldrich, France) solubilized in DMEM. BIOINK4 bioink was composed of 2% (w/v) fibrinogen, 2% (w/v) alginate and 5% (w/v) gelatin. BIOINK10 bioink was composed of 2% (w/v) fibrinogen, 5% (w/v) alginate and 5% (w/v) gelatin

Cells were trypsinized and seeded in each bioink as to obtain 2.10^6 cells.mL^{-1}, homogenized, loaded in a sterile 10cc syringe barrels (Nordson EFD, USA) and further incubated at 37°C for 15 minutes as described before[7]. No cell sedimentation was observed during this period, thanks to the viscosity of the bioink, leading to a homogeneous distribution of the cells within the cartridge. In order to stabilize bioink rheological properties, syringes were stored 30 minutes at 21°C before the extrusion experiments. Indeed, the bioink rheological properties (yield stress, viscosity) depend on the temperature. The 30 minutes incubation time therefore allows all of the bioink contained in the cartridge to reach the same properties.

2.3 Rheological characterization

A rotational stress-controlled rheometer (DHR2, TA instruments, USA) was used to define the rheological behaviour of the bioinks through the viscosity *vs* shear rate

curve. BIOINK4 and BIOINK10 were characterized with Peltier concentric cylinder (DIN rotor and standard cup) through a flow sweep procedure of shear rate scale [0.01; 1000] s^{-1} at 21°C, which was the microextrusion bioprinting temperature used.

2.4 Microextrusion bioprinting and control sample

Microextrusion was controlled using a high accuracy pressure delivery system (Ultimus V, Nordson EFD, USA). Tubular or conical nozzles were used with inner diameter ranging from 100 µm to 400 µm and length ranging from 6 mm to 13 mm (Optimum®, Nordson EFD, USA). All microextrusion experiments were performed at 21°C using a constant flow rate of 5 $\mu L.s^{-1}$ compatible with bioprinting[27,28]. According to the nozzle geometry, air pressure value was adjusted (***Supplementary material 1***) in order to maintain a constant flow rate. Bioink samples of 85 +- 25 µL were extruded in Eppendorf tubes of 1.5 ml loaded with 500 µl of labelling buffer (Annexin V: FITC Assay, BioRad, USA) pre-warmed at 37°.

2.5 Fibroblasts characterization after microextrusion

Following microextrusion, the bioink was completely dissolved by gentle homogenization and incubation at 37°C for 45 minutes in the labelling buffer (Annexin V: FITC Assay, BioRad, USA). Fibroblast populations were then characterized, numbered and classified in four categories: viable, lysed, apoptotic and necrotic. Cell population characterization and numbering assays were standardized with non-extruded sample controls.

Cell lysis was evaluated through standard cell counting using Malassez hematimeter. Several pictures of the Malassez grids were recorded for each conditions. A numerical post-treatment was performed using a home-made MATLAB® algorithm (***Supplementary material 2***) based on thresholding, segmentation and circular though transform methods to evaluate the total counts. Fibroblast viability rate was estimated as the difference between initial fibroblast population (before extrusion) and the lysed fibroblast population.

Apoptosis and necrosis were evaluated using flow cytometry (Becton Dickinson FACS Calibur Bdscience, USA). Annexin V-FITC/Propidium Iodide labelling kit (Annexin V: FITC Assay, BioRad, USA) was used to prepare the microextrusion samples prior analysis using CELLQuest 3 software (Bdscience, USA).

200 µL samples were analysed in triplicate through the acquisition of 1.10^4 corresponding events using the high-throughput sampler. Preliminary gating was carried out to target and discriminate freshly passaged fibroblast populations (99% viable). Similar preliminary gating was performed on a control sample of dissolved acellular bioink. Actinomycin D was used, as described in previous work[29], to gate the apoptotic signal and 3 freeze-thaw cycles were used on a fibroblast sample to gate the necrosis signal.

2.6 Flow properties simulation for microextrusion bioprinting

In order to study the flow behaviour through the tubular and conical nozzles, Computational Fluid Dynamics (CFD) simulations were performed on ANSYS FLUENT® 2020 R1 Academic. ANSYS FLUENT® is a commercial code which uses Finite Volume Method (FVM) to perform CFD calculations.

In order to reduce the computation time and make use of the axisymmetric property of the nozzle geometries (tubular, conical), a 2D axisymmetric space was used in the simulation. A steady, pressure-based solver was used with laminar flow model available in FLUENT®. This laminar flow model uses a modified form of mass and momentum conservation equations suitable for an axisymmetric geometry[30]. The mesh size of both nozzle geometries were maintained around 10 000 elements with refined mesh close to nozzle walls in order to capture the sharp velocity gradients near the walls. The viscous bioink behaviours were modelled with power law for non-Newtonian fluids given by Ostwald–de Waele relationship[31] ($k_{BIOINK4}$= 600; $k_{BIOINK10}$= 800 and $n_{BIOINK4}$ = $n_{BIOINK10}$ = 0.14) and having density of 1035 kg.m^{-3}. The range of shear rate ($\dot{\gamma}$) used was [0.1 to 100] s^{-1}. The boundary condition at the inlet was a constant flow rate of 5 µL.s^{-1}. The wall of the nozzle was provided with no-slip boundary condition. At the exit of the nozzle, a standard atmospheric pressure of 101 325 Pa was imposed.

The results of axial and radial velocity contours were obtained by solving the axial and radial momentum conservation equations for both tubular and conical nozzles with above mentioned boundary conditions. Data from bioink viscosity *vs* shear rate curves, cartridge and nozzle geometries, were integrated in FlowTips® Program (3d.FAB, France[32] to map the flow properties of bioink during microextrusion

experiments. FlowTips® uses an analytical approach based on Poiseuille equations to calculate shear rate, shear stress, axial and radial velocities.

2.7 Modelling of printing parameter impact on cell populations

The software SIMCA 15 (Umetrics, Sartorius) was used to perform data modelling thanks to Partial Least Square (PLS) approach. Partial least squares regression (PLS regression) is a statistical method based on principal components regression. It was used to find the multi-dimensional direction in the printing parameter dataset matrix which explain the maximal variance of the read-outs. Then, a linear regression model is found between the predicted read-outs and the measured read-outs by projecting them to a new space.

PLS models quality are evaluated on the basis of their number of component t[x], the value of the prediction error compared to the analytic ranges and the value of the linear regression coefficients R^2. Only R^2 coefficient higher than 0.7 are accepted as reliable regression models to predict datasets.

The dataset was pre-treated with a unit variance scaling. This step corresponds to calculating the standard deviation of each variable and obtaining a scaling weight as the inverse of the standard deviation. Variable values are then multiplied by this scaling weight in order to reach scaled variables which have all equal variance, i.e. the unit variance.

The PLS model robustness was analysed thanks to the stability of the linear regression coefficient R^2 after subtracting some samples to the dataset. This analysis is then called cross-validation and represented by the linear regression coefficient R^2_{CV}.

3. Results and discussion

Cell stress during microextrusion-based bioprinting is a well-known phenomenon and one can find in almost every bioprinting scientific articles a mention of this topic, usually under a live/dead experimental study. The classical approach being then empirical.

Herein, we are studying and solving the relationship between bioink rheology, flow rate distribution, nozzles geometries and cell fate after microextrusion. To do so, a bundle of rheological characterizations had to be performed, followed by flow simulation studies and calculation of shear stress and stress duration according to nozzle geometries. Then, fibroblast populations' fate (lysis, apoptosis and necrosis) were identified and correlated to the flow study results in order to identify the main key factors to guarantee a satisfactory cell viability rate in microextrusion-based bioprinting.

3.1 Flow study of bioinks

3.1.1 Rheological properties of bioinks

Successful microextrusion-based bioprinting, and more generally LDM-based 3D printing, are highly dependent upon the rheological properties of the deposited material, here the bioink. Indeed, properties such as static yield stress, shear thinning and thermosensitive viscosity are of upmost importance to guarantee the feasibility of the printing[6]. In order to modulate the bioink rheological behaviour, different formulations can be performed using the same three components, i.e. fibrinogen, alginate and gelatin. These biomolecules are the components of our already published bioink formulation[7] which rheological behaviour was shown to be mainly driven by the gelatin content (shear thinning and thermosensitive). In the present study, in order to generate two bioinks having similar rheological behaviours but slightly different viscosities, two compositions, BIOINK4 and BIOINK10, were selected. These two formulations were chosen to illustrate the impact of small viscosity variations upon cell fate.

The rheological characterizations of these two bioinks are presented in **Figure 1.** At low shear rate, between 1.10^{-2} and 4.10^{-2} s^{-1}, the shear stress (**Figure 1-A**) of both formulations seems constant, demonstrating a solid-like behaviour with static yield stresses of 100 Pa and 250 Pa for BIOINK4 and BIOINK10, respectively. This rheological behaviour is often sought during LDM-based 3D printing to maintain the shape of the bioprinted object during and after material deposition.

Beyond this low shear rate field, the applied shear stress is high enough to break physical networks and both bioinks behave as liquids and can be easily extruded. The viscosity (**Figure 1-B**) decreases then with increasing shear stress,

demonstrating a shear-thinning behaviour. Here, two domains can be observed. The first between 4.10^{-2} and 3.10^{1} s^{-1}, where the viscosity of BIOINK10 is greater than BIOINK4 (*e.g.* at 1 s^{-1}, $\eta_{BIOINK10}$ = 478 Pa.s^{-1} > $\eta_{BIOINK4}$ = 370 Pa.s^{-1}) but showing the same power law index ($n_{BIOINK10}$ = $n_{BIOINK4}$ = 0.14). Then around 5.10^{1} s^{-1}, the rheological behaviours change suddenly to reveal a second domain where the gelatin physical network is irreversibly disorganized.

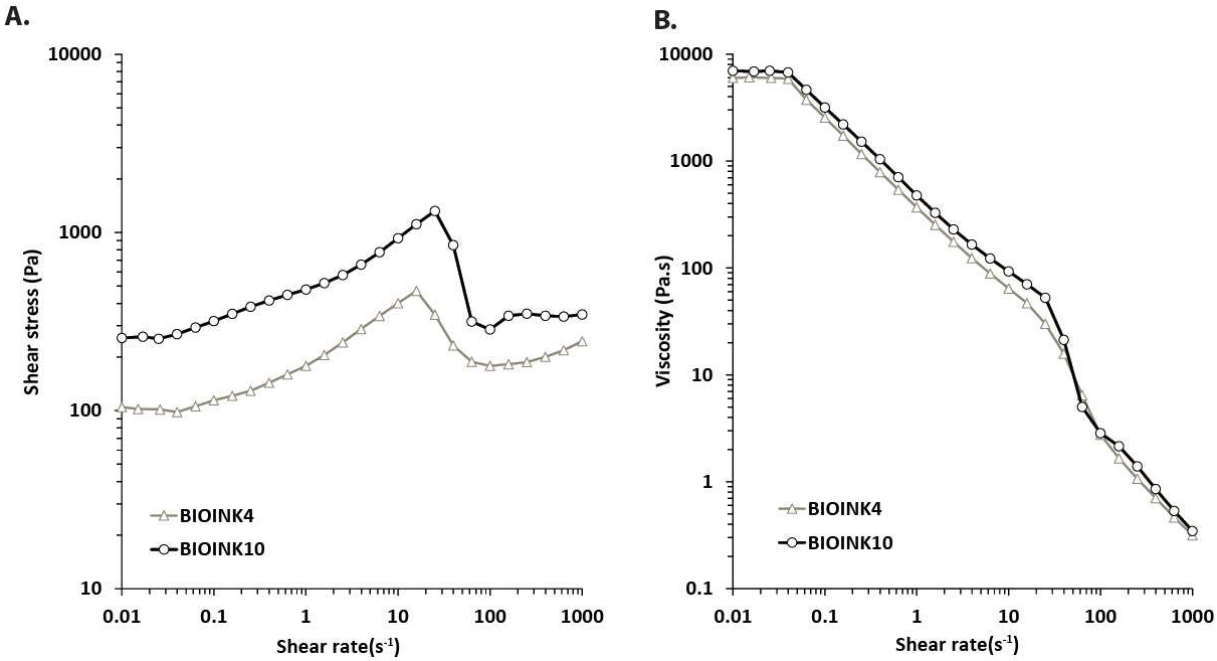

Figure 1: Rheological characterization of the selected BIOINK4 and BIOINK10 bioinks at 21°C. (A) Shear stress *vs* Shear rate of BIOINK4 and BIOINK10; (B) Viscosity *vs* Shear rate of BIOINK4 and BIOINK10. Results were obtained on three tests with less than 1% of standard deviation.

3.1.2 Flow simulation through nozzles

Once the two selected bioinks' rheological behaviours documented, their behaviour within the different bioprinting nozzles were simulated. Classical bioprinting nozzles [7] with diameter ranging from 100 µm to 400 µm and of various lengths were evaluated. CFD and Poiseuille equations-based simulation softwares (ANSYS® and FlowTip®) were used to predict the shear stress values and stress duration experienced by cells in the different nozzle geometries.

The simulated experiments consisted in extruding both bioinks with a constant flow rate set at 5 µL.s^{-1}. As expected using conical nozzles, radial and axial velocities co-exist and both increase while the nozzle diameter decreases (**Figure 2-A**). Maximal velocities are then reach by the end of the nozzle. On the contrary, in tubular

structures, the only existing velocity is the axial one, which remains constant throughout the nozzle length (**Figure 2-C**).

These velocity simulations were then complemented by the calculation of the shear stress distribution within the nozzle geometry. As presented in **Figure 2-B**, in the case of conical nozzle, shear stress value increases as a function of the position in the nozzle (length and radius), to reach a maximum value at the far end of the nozzle. Inversely, when using tubular structures (**Figure 2-D**), shear stress value increases only with the distance to the nozzle centre (Radius), whatever the positioning alongside the nozzle length.

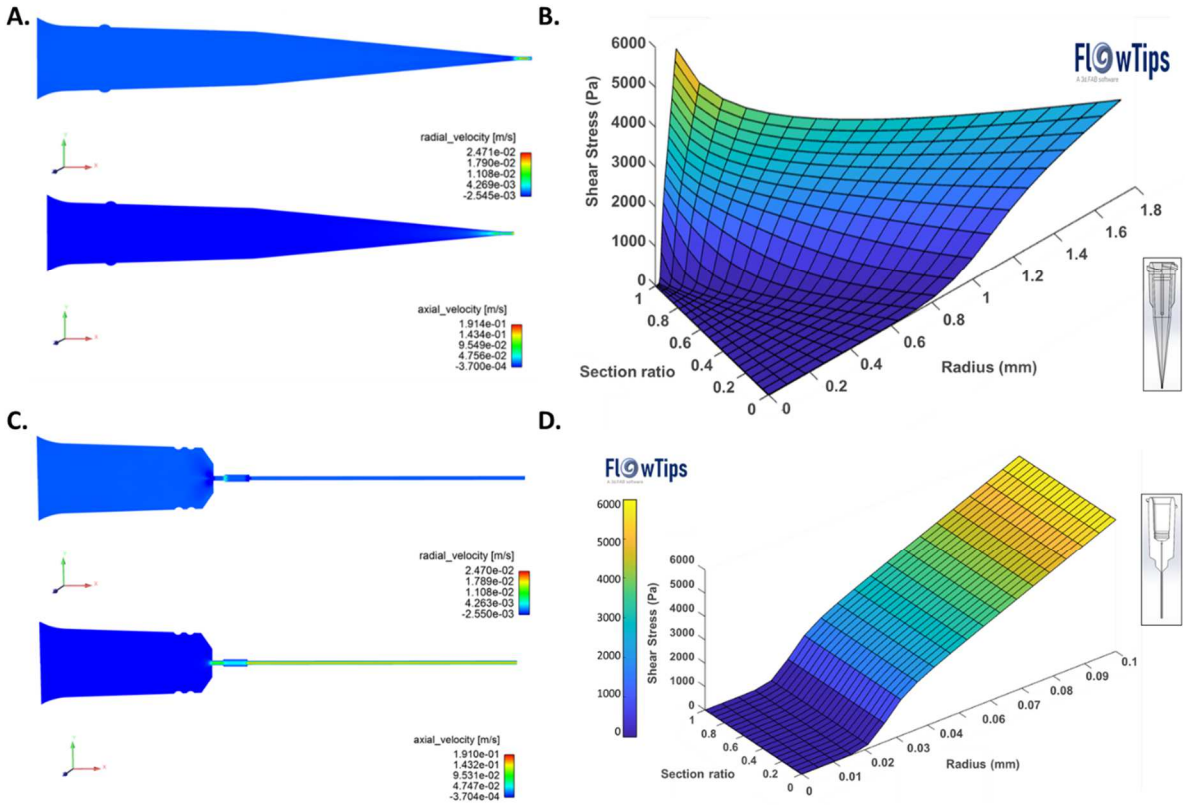

Figure 2: Examples of simulation data obtained using different nozzle geometries and BIOINK10 viscosity. (A) Simulation of Radial and Axial velocities of BIOINK10 through conical nozzle (D=200 µm, L=13 mm). (B) Simulation of shear stress values for BIOINK10 through conical nozzle (D=200 µm, L=13 mm) with a flow rate of 5 µL.s^{-1}. (C) Simulation of Radial and Axial velocities of BIOINK10 through tubular nozzle (D=200 µm, L=13 mm). (D) Simulation of shear stress values for BIOINK10 through tubular nozzle (D=200 µm, L=13 mm) with a flow rate of 5 µL.s^{-1}.

From both simulations, performed using a panel of nozzle geometries and our two selected bioinks, maximum wall shear stress values and residence times at wall within a given geometry were calculated (**Table 1**). Here, only the maximum wall shear stress values, and not the geometric distribution of the stress, were used as a

simplification of the system. Of course, this approach brings bias to the study since if the cell size (here approximately 30 µm for human fibroblast[33]) become negligible compared to the nozzle diameter, it is then unlikely that all studied cells experienced exactly the same shear stress and residence time. Nevertheless, when it comes to shear stress impact on living cells, it has been previously shown that the volume near the wall is the only position where cell damages are generated [14].

Using this simplification, for a particular bioink and when the nozzle diameter is constant, the nozzle geometry (conical or tubular) will not impact the value of the maximum wall shear stress ($\max(\tau_w)$) but only the residence time at wall (t). This is the case for example for BIOINK4 and 200 µm diameter nozzles for which $\max(\tau_w^{200\mu m,13mm})=\max(\tau_w^{200\mu m,6mm})=\max(\tau_w^{200\mu m,conical})$ whereas $t_{\max(\tau_w)}^{200\mu m,13mm} > t_{\max(\tau_w)}^{200\mu m,6mm} > t_{\max(\tau_w)}^{200\mu m,conical}$. Also, for a given bioink, the lower the nozzle diameter, the higher the maximum wall shear stress (*e.g.* BIOINK4: $\max(\tau_w^{400\mu m,6mm})>\max(\tau_w^{200\mu m,6mm})> \max(\tau_w^{100\mu m,6mm})$).

Then, increasing the bioink viscosity, from BIOINK4 to BIOINK10, results in an increasing of the maximum wall shear stress values (*e.g* $\max(\tau_{w,BIOINK10}^{200\mu m,6mm})>\max(\tau_{w,BIOINK4}^{200\mu m,6mm})$) without impacting residence time at wall ($t_{\max(\tau_w),BIOINK10}^{200\mu m,6mm} = t_{\max(\tau_w),BIOINK4}^{200\mu m,6mm}$ = 6.47 ms). This phenomenon is related to the fact that both bioinks have rheological properties (especially the power law index) close enough to lead to similar axial velocity[34] and then identical residence time at wall.

Table 1 : Stress-Time results in tubular and conical nozzles using BIOINK4 and BIOINK10 bioinks. Max τ_w: maximum wall shear stress within a given geometry. t: residence time at wall within a given geometry.

Nozzle	***400 µm conical***	***400 µm Tubular, length 6 mm***	***400 µm Tubular, length 13 mm***	***200 µm conical***	***200 µm Tubular, length 6 mm***	***200 µm Tubular, length 13 mm***	***100 µm conical***	***100 µm Tubular, length 6 mm***
CAD vision						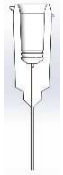		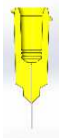

BIOINK4	$max(\tau_w)$ *(Pa)*	*3890*	*3890*	*3890*	*4789*	*4789*	*4789*	*5896*	*5896*
	t (ms)	*2.16*	*25.9*	*56.1*	*0.82*	*6.47*	*14.0*	*0.20*	*1.62*
BIOINK10	$max(\tau_w)$ *(Pa)*	*4619*	*4619*	*4619*	*5687*	*5687*	*5687*	*7002*	*7002*
	t (ms)	*2.16*	*25.9*	*56.1*	*0.82*	*6.47*	*14.0*	*0.20*	*1.62*

3.2 Cell populations' analysis

In order to fully characterize the cell fate following microextrusion, multiple techniques were used to quantify lysis, necrosis and apoptosis. It is indeed important to take into account all cell damage mechanisms (lysis, necrosis and apoptosis) to gain a deep understanding of the effect of the wall shear stress and residence time at wall.

First of all, the quality of the dissociated cellularized bioink was assessed by flow cytometry. **Figure 3-A** presents a typical cytogram obtained right after bioink dissociation. As can be seen, a clear partition between bioink debris and fibroblasts was obtained, proof that the sample preparation led to isolated single cells released from the initial bioink.

Then, cells were counted before and after extrusion in order to determine the population lysed directly during the bioprinting process. Here, a MATLAB® image analysis algorithm was developed to enumerate cells from hematimeter images (**Figure 3-B**). This approach was implemented in order to bring reproducibility (5%) to the counting step which variability is usually close to 15% when manual counting is performed[35].

The difference between the counted cells and the initial cell number enabled the calculation of the lysis percentage. Cytograms could have been used for direct counting of the lysed population but as can be seen in **Figure 3-A**, the results could have been partially bias by the presence of bioink debris.

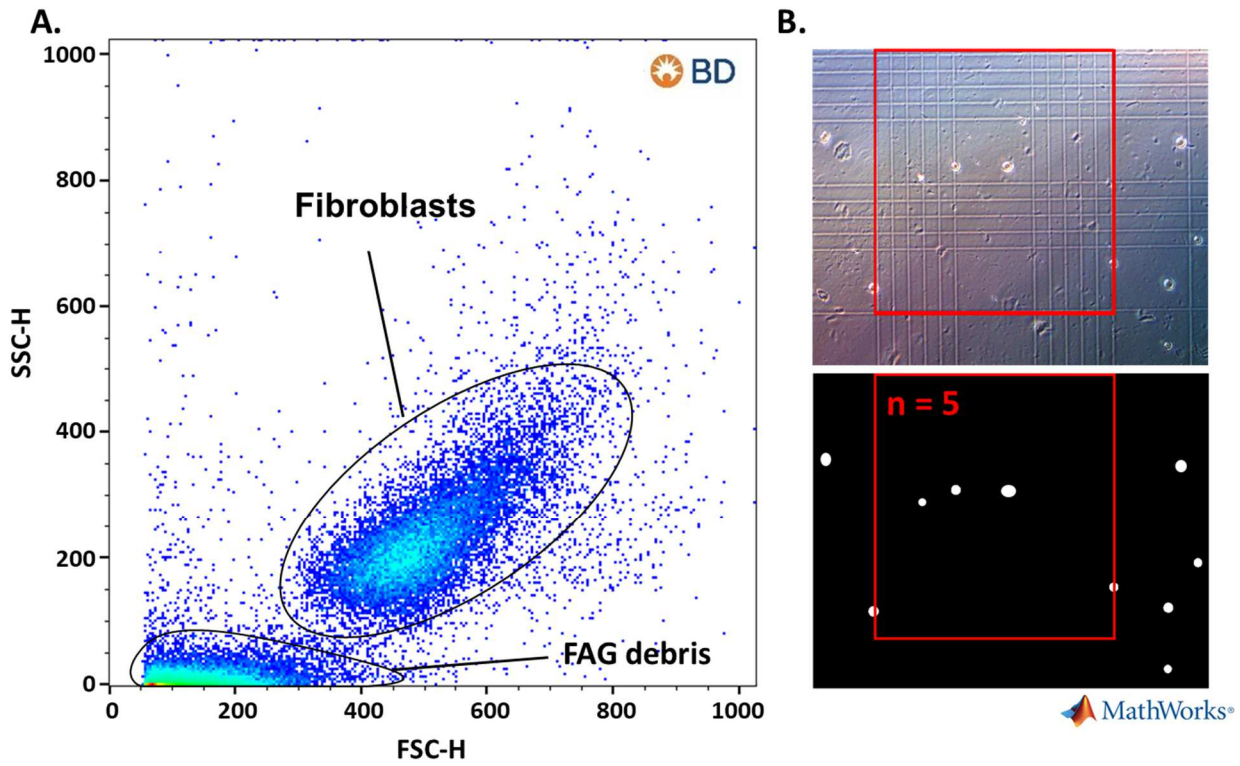

Figure 3 : Bioink dissociation and cell counting after microextrusion. (A) Cytogram of freshly dissociated fibroblast bioink (BIOINK10). Forward scatter (FSC-H) corresponds to cells size and side scatter (SSC-H) corresponds to cells granularity. (B) Example of the developed image analysis algorithm used for lysis percentage quantification (top: hematimeter image, bottom: processed image).

Finally, within the cells population which have maintained their integrity (not identified as lysed), cytometry with specific labelling using Annexin V and propidium iodide was used to identify apoptosis and necrosis sub-populations, respectively. Cells not being counted as lysed, necrotic or apoptotic were then considered as viable.

All results are presented in **Figure 4** for the two selected bioink formulations extruded using the different nozzle geometries.

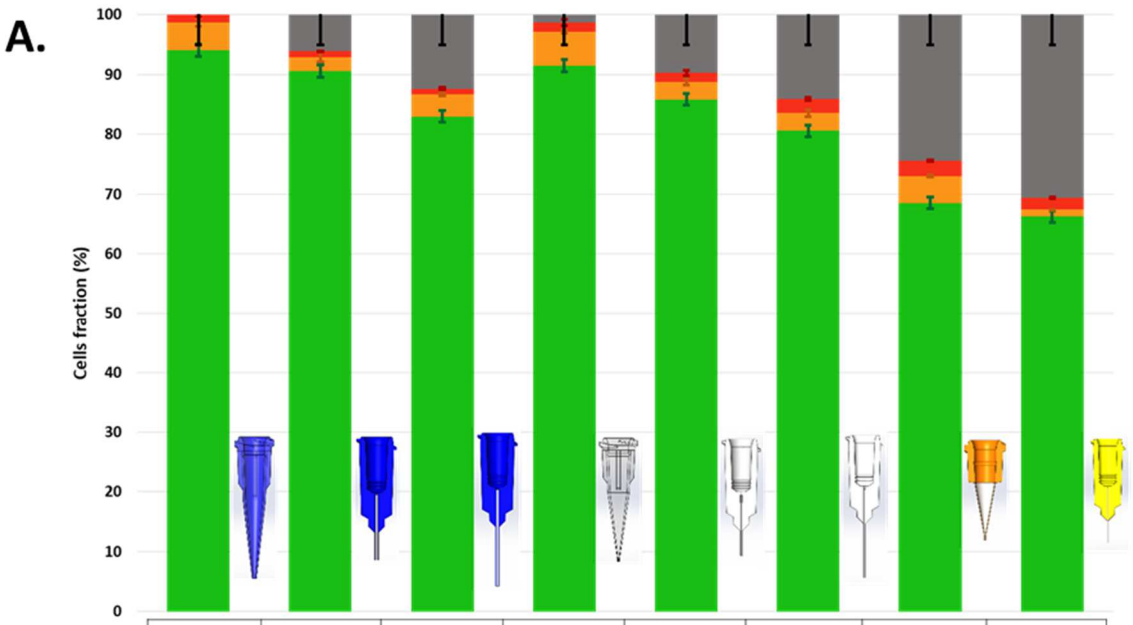

	400 µm conical	400 µm-Tubular, length 6mm	400 µm-Tubular, length 13mm	200 µm conical	200 µm-Tubular, length 6mm	200 µm-Tubular, length 13mm	100 µm conical	100 µm-Tubular, length 6mm
Lysis (%)	0 ± 0	6.1 ± 0.3	12.4 ± 0.6	1.3 ± 0.1	9.8 ± 0.5	14.1 ± 0.7	24.4 ± 1.2	30.6 ± 1.5
Necrotic (%)	1.3 ± 0.3	1 ± 0.1	0.9 ± 0.4	1.6 ± 1.0	1.4 ± 0.6	2.3 ± 0.5	2.5 ± 0.3	2.0 ± 0.3
Apoptotic (%)	4.6 ± 1.4	2.4 ± 1.6	3.7 ± 0.4	5.7 ± 0.5	3.0 ± 1.2	3.0 ± 1.0	4.5 ± 0.5	1.2 ± 0.2
Viable (%)	94 ± 4.7	90.5 ± 4.5	83 ± 4.2	91.4 ± 4.6	85.8 ± 4.3	80.6 ± 4.0	68.5 ± 3.4	66.2 ± 3.3

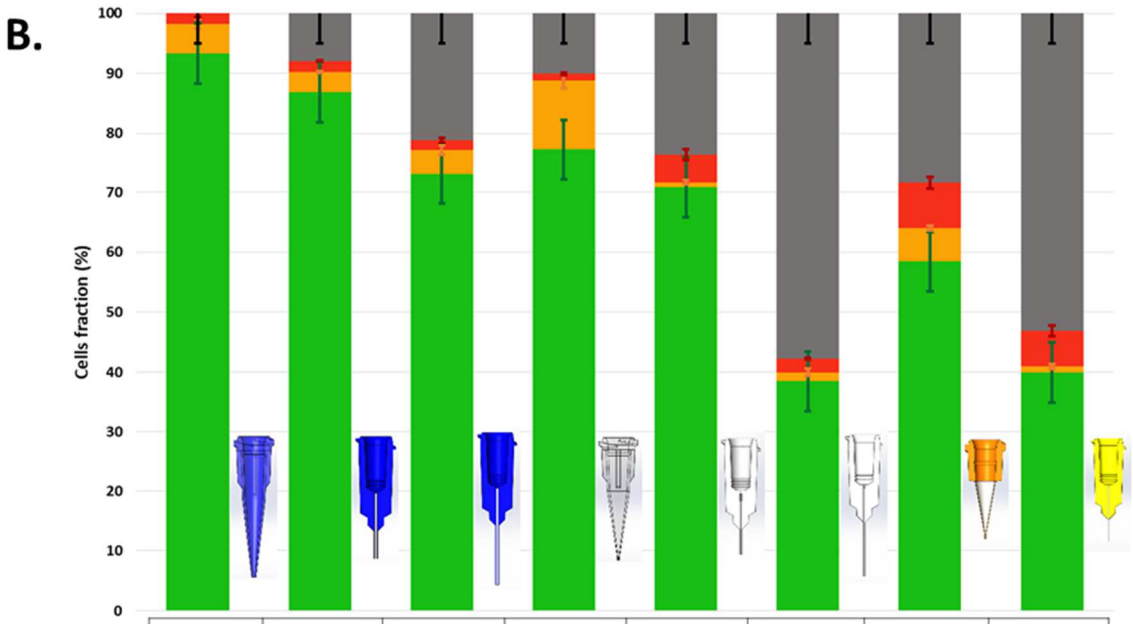

	400 µm conical	400 µm-Tubular, length 6mm	400 µm-Tubular, length 13mm	200 µm conical	200 µm-Tubular, length 6mm	200 µm-Tubular, length 13mm	100 µm conical	100 µm-Tubular, length 6mm
Lysis (%)	0 ± 0	7.9 ± 0.4	21.1 ± 1.1	10.1 ± 0.5	23.7 ± 1.2	57.8 ± 2.9	28.4 ± 1.4	53.2 ± 2.7
Necrotic (%)	1.8 ± 1	1.9 ± 0.2	1.9 ± 0.8	1.1 ± 0.3	4.6 ± 1.9	2.3 ± 0.3	7.6 ± 1.9	5.9 ± 1.8
Apoptotic (%)	4.9 ± 1.5	3.3 ± 0.3	3.9 ± 1.5	11.6 ± 2.4	0.8 ± 0.7	1.5 ± 1.2	5.6 ± 0.8	1.0 ± 0.8
Viable (%)	90.5 ± 4.7	86.9 ± 4.3	73.1 ± 3.7	77.2 ± 3.9	71.0 ± 3.5	38.5 ± 1.9	58.5 ± 2.9	39.9 ± 2.0

Figure 4: Cell populations' distribution according to bioink formulation and nozzle geometries. (A) Comparison of cell populations for different shapes, diameters and lengths of nozzles from extrusion using BIOINK4. (B) Comparison of cell populations for different shapes, diameters and lengths of nozzles from extrusion using BIOINK10. All data were obtained in triplicate at a constant flow rate of 5 µl.s^{-1}.

Analysing globally the obtained results bring us to the conclusion that at a constant flow rate, bioink rheological properties, nozzle diameter, length and shape have a direct impact on cell populations' distribution. Also, whatever the nozzle geometry, the viable fibroblasts' population is always higher for BIOINK4 than for BIOINK10. This behaviour was expected since BIOINK10 presents the higher viscosity, but the magnitude of the effect was surprising. Indeed, with only a 30% higher viscosity, the BIOINK10 led to drastic increases of the lysed populations. This lysed population difference reaching overwhelming 400% and 770% values for 200 µm-13 mm tubular and 200 µm conical nozzles, respectively.

Then, at constant residence time at wall (see **Table 1**), the higher the shear stress values, the lower the viable populations. Furthermore, at constant maximum wall shear stress, the longer the residence time at wall, the lower the viable populations.

Regarding the quantification of the damaged fibroblasts (lysis, necrosis and apoptosis) during the microextrusion, it is pretty clear that lysis seems to be the prevailing cell death pathway (oscillating between 0% and 53.2%) compared to necrosis and apoptosis (oscillating between 0.8% and 11.6%). Nevertheless, two exceptions were found for the 400 and 200 µm conical nozzles in which apoptotic cells for BIOINK4 were found to be the predominant damaged populations. The cells seem then to be protected from the wall shear stress. This observation might be the consequence of the presence, within the conical nozzles, of a velocity and shear stress gradient. We then hypothesized that the radial velocity, which only exists in conical nozzles, concentrates the fibroblasts at the centre of the nozzle, far from the wall. This phenomenon was previously illustrated for solid particles [36] and allows the cells to experience a shear stress weaker than the maximum wall shear stress value, leading then to a negligible population of lysed fibroblasts. Nevertheless, this assumption is limited to nozzle with diameter significantly higher that the fibroblast size. Indeed, in the case of the 100 µm conical nozzle, the fibroblast mobility toward the centre of the nozzle is constrained and the experienced shear stress is actually the maximum wall shear stress (lysis is then predominant within the damaged cell population).

3.3 Bioprinting cell viability awareness

In order to reach prediction of the impact of the bioprinting process on viable cell recovery (percentage of viable cells) and cell quality (viable, apoptotic, necrotic cell population), a partial least square (PLS) modelling approach was applied. Wall shear stress intensity, duration of the applied stress and bioink viscosity were used as model entries and biological events as predicted read-outs (viable, lysed, apoptotic and necrotic cell populations). In order to identify the printing parameter having the most important effect on cell viability, a preliminary Principal Component Analysis approach (PCA) was applied. This analysis of the complete dataset allowed us to identify wall shear stress as the most impacting parameter on the first PCA component t[1] (***Supplementary material 3***).

Then, PLS modelling was generated for each read-out sub-dataset. As can be seen in **Figure 5-Table**, viable cell population was correctly predicted with a high correlation (R^2 of 0.859; error of 9.2%) between predicted and measured viable cell percentage. On the contrary, necrotic and lysed onsets were described by a model but with unsatisfying R^2 of 0.695 and 0.677, respectively. Finally, in the case of the apoptotic onset, none of the pre-treatments or optimizations permitted to obtain an accurate model (R^2 below 0.7).

The only accurate model, describing the viable cell sub-dataset was then translated in the following equation 1:

$$V = 145.743 - 0.0133752 * \tau_w - 0.405308 * t + 0.00642919 * \eta$$

Equation 1 : Where V is the Viable cells ratio; τ_w the wall shear stress ; t the residence time and η the viscosity of bioink.

As a matter of fact, we were able to identify and model a clear link between viability rate and shear stress, stress time and viscosity. The predictability of this model was evaluated and is depicted in **Figure 5-B**. The model was shown to be predictive over a large range of cell viability (38.5 – 94%) with a prediction error of only 9.2%. This pave the way to further biomaterials (GelMa or nanocellulose-based bioinks) and printing conditions screening studies, allowing for a wider and discretised range of viscosity and shear duration. Indeed, additional datasets would undoubtedly allow to strengthen our present model but might also help reaching satisfactory modelling parameters for other cell populations (lysed, apoptotic, necrotic) not yet achieved. An additional perspective of our work would be to complement this study by integrating

the physiological inherent cell sensitivity to shear stress. This is planned as a next step by evaluating the impact of bioprinting process on several cell lines.

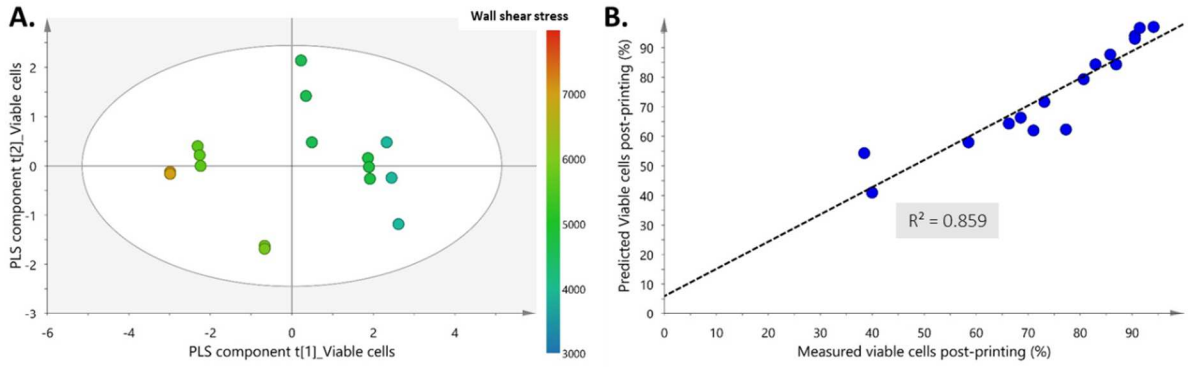

PLS predictive models	Correlation R^2	Correlation R^2 with cross-validation	Model PLS components	Analysis range (%)	Model Prediction error (%)
Viable cells	0.859	0.833	5	38.5 - 94	9.2%
Lysed cells	0.677	0.645	3	0 - 57.8	10.1%
Necrotic cells	0.695	0.49	3	0.51 - 7.38	1.2%
Apoptotic cells	-	-	-	-	-

Figure 5 : PLS analysis for predictive model study. (A) Score scatter plot of the viable cells dataset PLS analysis showing the impact of the wall shear stress on t[1] and t[2] components. (B) Correlation between the measured viable cells and the predicted viable cells using the developed model.

4. Conclusion

Viable and damaged fibroblast populations were evaluated after microextrusion through bioprinting using various nozzle geometries and bioink rheological properties. Four main observations can be extracted from this study. First, the viability rate decreases when the nozzle length or bioink viscosity increase. Second, the reduction of nozzle diameter decreases the viability rate. Third, the viability rate is higher in conical nozzles than in tubular nozzles. Fourth, lysis rate seems to be the prevailing cells death pathway compared to necrosis and apoptosis.

Understanding and mastering precisely the shear generated during the microextrusion bioprinting process is therefore essential but, in view of the multitude of available bioinks and printing parameters used in microextrusion bioprinting, this systematic approach could be limited, time-consuming and expensive. For example, fibroblasts' viability was found to drop below 80% for shear stress more than 5000 Pa over a duration of 30 ms. These results are in accordance with previously published results [12],[14]. More recently, Muller reported that a maximum shear stress value of 160 Pa was detrimental to chondrocyte viability[37]. These studies suggest then that each cell type has a different resistance to shear and that in order to accurately predict particular cell viability, it is necessary to evaluate the shear resistance profile of each cell line.

In the present study and for the first time in the bioprinting field, flow simulation and cells' fate results were used to establish a Viability-Stress-Time-Viscosity mathematical relationship. This model was shown to be highly accurate to predict the viable cell recovery rate, whatever the bioprinting set-up geometry. Nevertheless, in our actual prediction system, assumption was made about cells' distribution within the nozzle and we hypothesized that the radial velocity, which only exists in conical nozzles, concentrates the fibroblasts at the centre of the nozzle, far from the wall. To go one step further in the prediction, using microfluidic systems[38] of controlled geometry shall, in the near future, bring new insights about cell fate within bioprocess implementation protocols.

References

1. Levato R, Jungst T, Scheuring RG, Blunk T, Groll J, Malda J. From Shape to Function: The Next Step in Bioprinting. *Adv Mater*. 2020;32(12). doi:10.1002/adma.201906423

2. Bishop ES, Mostafa S, Pakvasa M, et al. 3-D bioprinting technologies in tissue engineering and regenerative medicine: Current and future trends. *Genes Dis*. 2017;4(4):185-195. doi:10.1016/j.gendis.2017.10.002

3. Duchamp M, Liu T, van Genderen AM, et al. Sacrificial Bioprinting of A Mammary Ductal Carcinoma Model. *Biotechnol J*. Published online 2019:e1700703. doi:10.1002/biot.201700703

4. Palareti G, Legnani C, Cosmi B, et al. Comparison between different D-Dimer cutoff values to assess the individual risk of recurrent venous thromboembolism: Analysis of results obtained in the DULCIS study. *Int J Lab Hematol*. 2016;38(1):42-49. doi:10.1111/ijlh.12426

5. Echave MC, Hernáez-Moya R, Iturriaga L, et al. Recent advances in gelatin-based therapeutics. *Expert Opin Biol Ther*. 2019;0(0):14712598.2019.1610383. doi:10.1080/14712598.2019.1610383

6. Sigaux N, Pourchet L, Breton P, Brosset S, Louvrier A, Marquette CA. 3D Bioprinting:principles, fantasies and prospects. *J Stomatol Oral Maxillofac Surg*. 2019;120(2):128-132. doi:10.1016/j.jormas.2018.12.014

7. Pourchet LJ, Thepot A, Albouy M, et al. Human Skin 3D Bioprinting Using Scaffold-Free Approach. *Adv Healthc Mater*. 2017;6(4):1-8. doi:10.1002/adhm.201601101

8. Foyt DA, Norman MDA, Yu TTL, Gentleman E. Exploiting Advanced Hydrogel Technologies to Address Key Challenges in Regenerative Medicine. *Adv Healthc Mater*. 2018;7(8). doi:10.1002/adhm.201700939

9. Szojka A, Lalh K, Andrews SHJ, Jomha NM, Osswald M, Adesida AB. Derakhshanfar. *Bioprinting*. 2017;8(April):1-7. doi:10.1016/j.bprint.2017.08.001

10. Seol YJ, Lee H, Copus JS, et al. 3D bioprinted biomask for facial skin

reconstruction. *Bioprinting*. 2018;10. doi:10.1016/j.bprint.2018.e00028

11. Cidonio G, Glinka M, Dawson JI, Oreffo ROC. The cell in the ink: Improving biofabrication by printing stem cells for skeletal regenerative medicine. *Biomaterials*. 2019;209(March):10-24. doi:10.1016/j.biomaterials.2019.04.009

12. Webb B, Doyle BJ. Parameter optimization for 3D bioprinting of hydrogels. *Bioprinting*. 2017;8:8-12. doi:10.1016/j.bprint.2017.09.001

13. Choonara YE, Du Toit LC, Kumar P, Kondiah PPD, Pillay V. 3D-printing and the effect on medical costs: A new era? *Expert Rev Pharmacoeconomics Outcomes Res*. 2016;16(1):23-32. doi:10.1586/14737167.2016.1138860

14. Blaeser A, Duarte Campos DF, Puster U, Richtering W, Stevens MM, Fischer H. Controlling Shear Stress in 3D Bioprinting is a Key Factor to Balance Printing Resolution and Stem Cell Integrity. *Adv Healthc Mater*. 2016;5(3):326-333. doi:10.1002/adhm.201500677

15. Koch F, Tröndle K, Finkenzeller G, Zengerle R, Zimmermann S, Koltay P. Generic method of printing window adjustment for extrusion-based 3D-bioprinting to maintain high viability of mesenchymal stem cells in an alginate-gelatin hydrogel. *Bioprinting*. Published online August 1, 2020:e00094. doi:10.1016/j.bprint.2020.e00094

16. Bin and Feng Lu WSJ and WB and HLS and SJ and S. Shear stress analysis and its effects on cell viability and cell proliferation in drop-on-demand bioprinting. *Biomed Phys Eng Express*. 2018;4.

17. Giuseppe M Di, Law N, Webb B, et al. Mechanical behaviour of alginate-gelatin hydrogels for 3D bioprinting. *J Mech Behav Biomed Mater*. 2018;79:150-157. doi:10.1016/j.jmbbm.2017.12.018

18. Munir N, Larsen RS, Callanan A. Fabrication of 3D cryo-printed scaffolds using low-temperature deposition manufacturing for cartilage tissue engineering. *Bioprinting*. 2018;10:e00033. doi:10.1016/j.bprint.2018.e00033

19. Gillispie GJ, Han A, Uzun-per M, et al. The Influence of Printing Parameters and Cell Density on Bioink Printing Outcomes. Published online 2020:1-28. doi:10.1089/ten.TEA.2020.0210

20. Born C, Thomas CR. Estimation of Disruption of Animal Cells by Laminar Shear Stress. Published online 1992.

21. Nair K, Gandhi M, Khalil S, et al. Characterization of cell viability during bioprinting processes. *Biotechnol J*. 2009;4(8):1168-1177. doi:10.1002/biot.200900004

22. Nerem RM. Shear force and its effect on cell structure and function. *ASGSB Bull*. 1991;4(2):87-94. http://www.ncbi.nlm.nih.gov/pubmed/11537186

23. White CR, Frangos JA. The shear stress of it all : the cell membrane and mechanochemical transduction. 2007;(June):1459-1467. doi:10.1098/rstb.2007.2128

24. Ho L, Hsu S hui. Cell reprogramming by 3D bioprinting of human fibroblasts in polyurethane hydrogel for fabrication of neural-like constructs. *Acta Biomater*. 2018;70:57-70. doi:10.1016/j.actbio.2018.01.044

25. Zhao Y, Li Y, Mao S, Sun W, Yao R. The in fl uence of printing parameters on cell survival rate and printability in microextrusion-based 3D cell printing technology. *Biofabrication*. 7(4):45002. doi:10.1088/1758-5090/7/4/045002

26. Kiyotake EA, Douglas AW, Thomas EE, Michael S. Development and Quantitative Characterization of the Precursor Rheology of Hyaluronic acid Hydrogels for Bioprinting. *Acta Biomater*. Published online 2019. doi:10.1016/j.actbio.2019.01.041

27. Ozbolat IT, Chen H, Yu Y. Development of “Multi-arm Bioprinter” for hybrid biofabrication of tissue engineering constructs. *Robot Comput Integr Manuf*. 2014;30(3):295-304. doi:10.1016/j.rcim.2013.10.005

28. Fisch P, Holub M, Zenobi-Wong M. Improved accuracy and precision of bioprinting through progressive cavity pump-controlled extrusion. *bioRxiv*. 2020;(Xxxx):2020.01.23.915868. doi:10.1101/2020.01.23.915868

29. Schmid I, Uittenbogaart C, Jamieson BD. Live-cell assay for detection of apoptosis by dual-laser flow cytometry using Hoechst 33342 and 7-amino-actinomycin D. 2007;2(1):187-190. doi:10.1038/nprot.2006.458

30. Ansys Fluent Theory Guide, Chapter 1, Page No: 2,3. 2017;(January).

31. Ostwald W. About the rate function of the viscosity of dispersed systems. 1925;36:99– 117.

32. Lemarié L, Courtial E-J. FlowTips: Predictive tool for bioprinting – 3d.FAB. Accessed September 1, 2020. http://fabric-advanced-biology.univ-lyon1.fr/flowtips/

33. Grinnell F, Ho C, Tamariz E, Lee DJ, Skuta G. Dendritic Fibroblasts in Three-dimensional Collagen Matrices. 2003;14(February):384-395. doi:10.1091/mbc.E02

34. Fulchiron R, K BS, Carrot C. Extrudate swell and isothermal melt spinning analysis of linear low density polyethylene using the Wagner constitutive equation. 1997;69.

35. Nielsen LK, Smyth GK, Greenfield PF. Hemacytometer Cell Count Distributions: Implications of Non-Poisson Behavior. *Biotechnol Prog*. 1991;7(6):560-563. doi:10.1021/bp00012a600

36. Quan Z, Wu A, Keefe M, et al. Additive manufacturing of multi- directional preforms for composites : opportunities and challenges. *Biochem Pharmacol*. 2015;18(9):503-512. doi:10.1016/j.mattod.2015.05.001

37. Müller M, Öztürk E, Arlov Ø, Gatenholm P, Zenobi-Wong M. Alginate Sulfate–Nanocellulose Bioinks for Cartilage Bioprinting Applications. *Ann Biomed Eng*. 2017;45(1):210-223. doi:10.1007/s10439-016-1704-5

38. Urbanska M, Muñoz HE, Bagnall JS, et al. high-throughput cell deformability measurements. doi:10.1038/s41592-020-0818-8